PASJ: Publ. Astron. Soc. Japan **53**, 305–314, 2001 April 25

SiO Maser Survey of Southern IRAS Sources

Shuji DEGUCHI
Nobeyama Radio Observatory, National Astronomical Observatory,
Minamimaki, Minamisaku, Nagano 384-1305
deguchi@nro.nao.ac.jp
Jun-ichi NAKASHIMA
Department of Astronomical Science, The Graduate University for Advanced Studies
Minamimaki, Minamisaku, Nagano 384-1305
and
Ramesh BALASUBRAMANYAM[1]
School of Physics, University of New South Wales, Sydney, NSW 2052, Australia

(Received 2000 October 23; accepted 2001 February 19)

Abstract

We have surveyed 163 southern IRAS sources in the SiO $J = 2$–1 $v = 1$ maser line at 86 GHz, obtaining 38 (22 new and 16 previously known) detections. These detections include 6 stars not previously detected in OH 1612 MHz surveys, and 4 sources assigned incorrect OH radial velocities. The distance reachable in this survey turned out to be about 4 kpc. The local velocity dispersion near the Sun were found to be approximately 30 km s^{-1} for these IRAS/SiO sources. A relatively high concentration of the SiO detected sources were found at the area $320^\circ < l < 340^\circ$ (toward "Norma tangent"). The estimated distances for these sources suggest that this concentration is spread between 2 and 6 kpc from the Sun, peaking on the Scutum–Crux arm.

Key words: Galaxy: kinematics and dynamics — Galaxy: structure — radio lines: stars — stars: late-type

1. Introduction

Stellar maser sources are good tracers of the galactic structure (Izumiura et al. 1995, 1999; Sevenster et al. 1997ab; Deguchi et al. 2000a). Radio line observations provide an accurate radial-velocity dataset, while infrared continuum observations provide distances to the sources, both fundamental for studying galactic dynamics. Though extensive surveys in SiO maser lines have been performed for southern objects (Allen et al. 1989; Deguchi et al. 1990; Haikala 1990; Hall et al. 1990; Haikala et al. 1994; Nyman et al. 1998), the number of SiO detected sources is still less than 150. This is much smaller than the number of objects detected in northern surveys ($\sim$ 1000). Because these southern surveys covered all sources with $\delta < 0^\circ$, they should have a comparable number of (or more) detections, if the same survey depth were reached (though a simple comparison is somewhat questionable). The depths of these southern surveys are within a few kpc from the Sun. This is still not sufficiently deep compared with the corresponding surveys in the northern sky, which were made mostly with the Nobeyama 45-m telescope reaching to 12 kpc (Izumiura et al. 1999; Deguchi et al. 2000ab). Galactic structure studies suffer an imbalance owing to this shallowness of the surveys in the south, and attempts to remedy this situation are important.

In order to improve the southern SiO maser dataset, we have made an SiO $J = 2$–1 $v = 1$ line survey of southern IRAS sources with the 22-m telescope at the Mopra Observatory, Australia. Recently, the outer panels of the dish were replaced to make the entire 22-m dish to reflect mm-waves; the surface was also re-adjusted to obtain an improved aperture efficiency of about 30%. We used this upgraded mm-wave telescope for surveying color-selected IRAS sources. We observed 163 sources and detected the SiO line in 38. We present here the results of these observations.

2. Observations

The observations in the SiO $J = 2$–1 $v = 1$ transition at 86.243 GHz were made during 2000 July 5–14 with the ATNF Mopra 22-m telescope in Australia using a cooled dual-polarization SIS mixer receiver. During the first half of the observing run, one channel (A) was tuned to CO at 115.271 GHz and the other (B) to SiO at 86.243 GHz. During the second half of the observing run, both channels were tuned to SiO at 86.243 GHz. However, the first receiver (A) was not well optimized for SiO observations at 86 GHz, and therefore that data could not be added to the second channel data to improve the sensitivity. For the second channel (B), the DSB[2] system temperature was approximately 160–200 K at 86 GHz (including atmospheric attenuation and propagation losses), and the SSB system temperature for the first channel (A) was 450–600 K at 115 GHz. The observations were made with the 1024-channel autocorrelator spectrometers with a bandwidth coverage of 64 MHz. This resulted in a velocity coverage of about 200 km s^{-1} with a resolution of 0.2 km s^{-1} per channel. The center velocity of the spectrometer was

[1] Permanent address: Raman Research Institute, Bangalore 560080, India.

[2] The center frequency of the lower side band is 83.4 GHz, presuming that no strong line contaminates the SiO line in the upper side band.

Table 1. List of detections.

IRAS name	Obs. date	V_{lsr}	T_a^{peak}	Integr. int.	T_{rms}	V_{star} (mol.)	Reference*
	(yymmdd.d)	(km s^{-1})	(K)	(K km s^{-1})	(K)	(km s^{-1})	
03074−8732	000712.9	7.3	0.146	0.352	0.044	12.0 (CO,SiO)	1,2
03336−7636	000712.9	2.0	0.174	0.378	0.026	0.1 (OH,SiO)	2,7
04140−8158	000705.9	21.1	0.693	3.277	0.047	17.0 (OH,SiO)	1,2,7
04404−7427	000705.0	−11.3	1.383	2.012	0.052	−12.2 (OH,SiO)	2,7
05027−2158	000707.0	−27.2	0.554	1.496	0.052	−8.1 (OH,SiO)	4,7
05098−6422	000706.0	31.5	0.653	1.935	0.050	32.4 (OH,SiO)	2,3,7
05345−4406	000707.1	17.1	0.208	0.431	0.028	18.8 (OH)	7
09027−2758	000713.1	91.0	0.106	0.490	0.045	89.1 (OH)	7
09503−5439	000711.2	−64.0	0.068	0.169	0.014	—	7
10495−5815	000713.2	−15.9	0.077	0.419	0.021	7.5 (OH)	7
13203−5536	000713.2	−7.2	0.134	0.304	0.027	−43.2 (OH,SiO)	2,7
14477−5812	000713.3	3.1	0.124	0.435	0.023	16.0 (OH)	6
15155−5723	000709.3	−11.1	0.220	0.542	0.043	−8.7 (OH)	6
15229−5445	000712.5	−18.1	0.166	0.383	0.025	−22.0 (OH)	6
15509−5207	000708.3	−52.2	0.188	0.501	0.043	−50.5 (OH)	6
15541−5408	000708.4	−75.1	0.234	0.166	0.044	−70.9 (OH)	6
16005−4126	000712.5	−66.5	0.111	0.269	0.022	—	7
16077−5830	000710.5	−41.3	0.314	0.507	0.049	−59.8 (OH)	7
16219−5048	000708.4	−54.7	0.157	0.253	0.042	−50.5 (OH,SiO)	2,6
16327−4848	000711.5	−64.6	0.095	0.350	0.027	−71.6 (OH)	6
16589−3315	000708.5	0.4	0.209	0.375	0.038	−1.4 (OH,SiO)	5,7
17122−2707	000708.6	−13.8	0.219	0.253	0.040	−15.5 (OH,SiO)	5,7
17131−6225	000708.7	−59.8	0.457	0.821	0.053	—	7
17319−6234	000708.6	−8.3	0.414	0.858	0.044	−7.2 (OH)	7
17368−3000	000710.6	5.1	0.151	0.431	0.031	13.3 (OH)	7
18467−4802	000710.7	49.0	0.233	0.258	0.050	47.8 (OH)	7
20042−4241	000710.7	−23.2	0.226	0.713	0.053	−34.0 (SiO)	1,4,7
20111−4708	000706.8	7.1	0.402	0.778	0.043		
20135−7152	000708.8	−1.1	0.799	1.210	0.050	−3.0 (OH,SiO)	1,2,7
20171−5620	000713.7	−45.3	0.139	0.199	0.029		
20296−2151	000708.8	7.2	0.233	0.381	0.051	7.5 (OH)	7
20343−3020	000708.8	−24.1	0.258	0.438	0.053	−24.1 (OH)	7
20484−7202	000705.7	−31.6	0.240	0.535	0.031	—	7
20526−5431	000705.8	31.5	0.264	0.666	0.058	28.4 (SiO)	2,7
20541−6549	000708.8	−5.0	0.564	1.404	0.047	−18.0 (SiO)	2
20571−3706	000708.9	−12.0	0.120	0.247	0.027	−17.5 (OH)	7
21069−3843	000706.8	−23.3	0.877	0.989	0.049	−23.0 (SiO)	4,7
22230−4841	000706.9	−28.9	0.399	0.558	0.047	−25.9 (SiO)	4

* References: 1. Deguchi et al. (1990), 2. Haikala (1990), 3. Hall et al. (1990), 4. Haikala et al. (1994), 5. Izumiura et al. (1995), 6. Sevenster et al. (1997b), 7. te Lintel-Hekkert et al. (1990); References 1–5 are SiO maser observations, while references 6 and 7 are OH 1612 MHz observations. The previously known SiO detections are in the rows which contain references 1–5, or are indicated by "SiO" in the 7th column. References 3 and 5 are the SiO J = 1–0 v = 1 or 2 observations, and others are the SiO J = 2–1 v = 1 observations.

shifted by a few 10 km s^{-1} to allow for galactic rotation, depending on the position and distance to the source. The telescope aperture efficiency was approximately 30%, implying a conversion factor for antenna temperature to flux density scale of about 25 Jy K^{-1}. All of the observations were made in the position-switching mode with an off position of about 3′ separation. The integration time was typically about 15 min, and more integrations were made when a weak signal was seen. The pointing was carefully checked about every hour using bright known SiO maser sources; the average pointing accuracy was about 10″ (rms). The half-power beam width of the telescope was about 36″.

The source selection was made in terms of the IRAS 12 μm flux density (above 10 Jy), the colors, $C_{12} = \log(F_{25}/F_{12})$ and $C_{23} = \log(F_{60}/F_{25})$, and variability index (above 95). In the present survey, we took the sources in the following color ranges; $-0.4 < C_{12} < 0.4$, and $-1 < C_{23} < 0.1$. It is known that dusty late-type stars with SiO masers are effectively picked up with these selection criteria (Izumiura et al. 1994). The IRAS variability index can be used to

Table 2. List of nondetections.

IRAS name	T_{rms} (K)	Obs. date (yymmdd.d)	IRAS name	T_{rms} (K)	Obs. date (yymmdd.d)	IRAS name	T_{rms} (K)	Obs. date (yymmdd.d)
02234−0024	0.027	000711.7	15004−5809	0.041	000709.3	17076−4702	0.044	000710.6
02238−5947	0.026	000711.8	15044−5822	0.033	000713.3	17099−3904*	0.047	000706.6
03274−5608	0.026	000712.9	15082−5600	0.041	000713.4	17132−5003	0.044	000706.6
04046−5458	0.030	000713.0	15086−5613	0.044	000705.4	17146−4158	0.037	000712.7
04311−0004	0.030	000711.8	15174−4821	0.043	000713.4	17177−3627	0.033	000712.7
04505−1006	0.025	000711.8	15225−5605	0.035	000706.5	17186−4208	0.046	000711.6
05096−4834	0.027	000713.0	15230−5538	0.046	000713.4	17189−6501	0.022	000713.7
05150−4056	0.025	000711.9	15246−5658	0.051	000708.2	17210−3946	0.046	000711.6
05363−5540	0.021	000713.0	15254−7718	0.042	000709.4	17243−3724	0.046	000706.6
05418−5058	0.046	000706.0	15272−5223	0.056	000713.4	17262−5003	0.050	000708.7
08089−3511	0.042	000712.0	15338−5236	0.045	000713.4	17264−3521	0.045	000711.6
08098−4547	0.031	000712.0	15356−6722	0.047	000708.3	17288−3748	0.040	000708.5
08360−5723	0.028	000713.0	15357−5239	0.041	000713.5	17317−4153	0.047	000711.6
09072−5933	0.266	000706.2	15366−5811	0.045	000713.5	17353−3856	0.042	000711.7
09089−2149	0.174	000713.1	15413−6518	0.058	000713.5	17375−3652	0.056	000708.7
09118−5333	0.051	000706.2	15422−4414	0.046	000713.5	17401−5730	0.045	000706.7
09317−5116	0.029	000712.1	15474−5223	0.045	000708.3	17453−3340	0.040	000710.6
09418−5842	0.029	000712.1	16030−5928	0.076	000710.4	17517−3339	0.041	000710.6
09425−6040	0.043	000705.2	16055−4621	0.044	000708.4	17534−3030	0.044	000709.4
09526−5701	0.059	000706.2	16064−4200	0.043	000709.4	17547−3249	0.037	000710.6
10311−5506	0.057	000706.3	16119−3811	0.043	000713.6	18095−1813*	0.042	000706.7
10338−5139	0.029	000712.2	16146−5257	0.039	000708.4	18122−1818*	0.044	000705.5
10389−5306	0.029	000712.2	16156−4756	0.061	000710.5	18491−3648	0.046	000706.7
11038−5817	0.087	000707.1	16156−5613	0.099	000710.5	18498−0017*	0.046	000705.6
11152−6709	0.040	000709.2	16178−4625	0.046	000713.5	20078−5534	0.033	000712.7
11244−5835	0.112	000707.2	16199−5056	0.044	000713.5	20150−5246	0.044	000713.7
11316−5926	0.046	000711.3	16265−5100	0.040	000710.4	20168−7849	0.048	000705.6
11333−5752	0.042	000709.2	16279−5342	0.040	000708.4	20259−4035	0.046	000706.8
11418−6706	0.027	000713.1	16320−4419	0.039	000710.4	20372−3948	0.048	000713.7
11453−6111	0.043	000709.2	16337−4525	0.037	000712.6	20500−7509	0.046	000713.7
12162−5921	0.048	000711.3	16391−4634	0.039	000708.5	21046−2407	0.045	000712.8
12419−6058	0.027	000713.2	16399−3548	0.041	000709.4	21206−4054	0.032	000710.7
13255−6102	0.061	000708.2	16414−4941	0.050	000709.5	21284−0747	0.063	000710.8
14086−6907	0.032	000712.5	16434−4351	0.042	000712.6	21453−4708	0.040	000705.8
14119−6453	0.177	000708.2	16446−4243	0.058	000706.5	22009−2817	0.041	000712.8
14135−6257	0.050	000711.5	16528−4059	0.047	000706.6	22023−5614	0.041	000705.8
14169−6529	0.058	000712.2	16557−4531	0.042	000708.5	22189−6107	0.045	000705.8
14297−6010	0.036	000712.2	16567−4659	0.152	000709.6	22231−4529	0.070	000706.9
14310−7703	0.045	000705.4	17010−3840	0.054	000706.6	22479−7934	0.029	000710.7
14425−6023*	0.044	000713.3	17030−4246	0.052	000712.6	23206−6638	0.031	000709.0
14428−5742	0.031	000713.3	17055−3753	0.049	000710.5	23548−6539	0.043	000709.0
14481−6054	0.046	000712.5	17059−3550	0.032	000712.7			

* Indicates candidates for proto-planetary nebulae.

choose Asymptotic Giant Branch (AGB) stars in the bright IRAS sample (Allen et al. 1993). In addition to the normal dust-enshrouded late-type stars, we selected a few sources which exhibit the color of planetary nebulae ($C_{12} \sim 0.5$ and $C_{23} \sim 0.7$), hoping that some might exhibit maser emission like that found in a protoplanetary nebula with that color, IRAS 19312+1950 (Nakashima, Deguchi 2000). The IRAS variability indices are below 30 for these sources.

We detected SiO maser emission in 38 sources among the 163 IRAS sources observed. Of these, 22 were new detections in SiO, and 16 were previously known SiO detections. The results are summarized in table 1 for detections and table 2 for nondetections. The observed positions were those given in the IRAS Point Source Catalog (Beichman et al. 1988); they are sufficiently accurate ($\sim 10''$–$20''$) when compared with the telescope beam size.

The last two columns in table 1 summarize the previous observations in OH or SiO (if both unavailable, CO data were

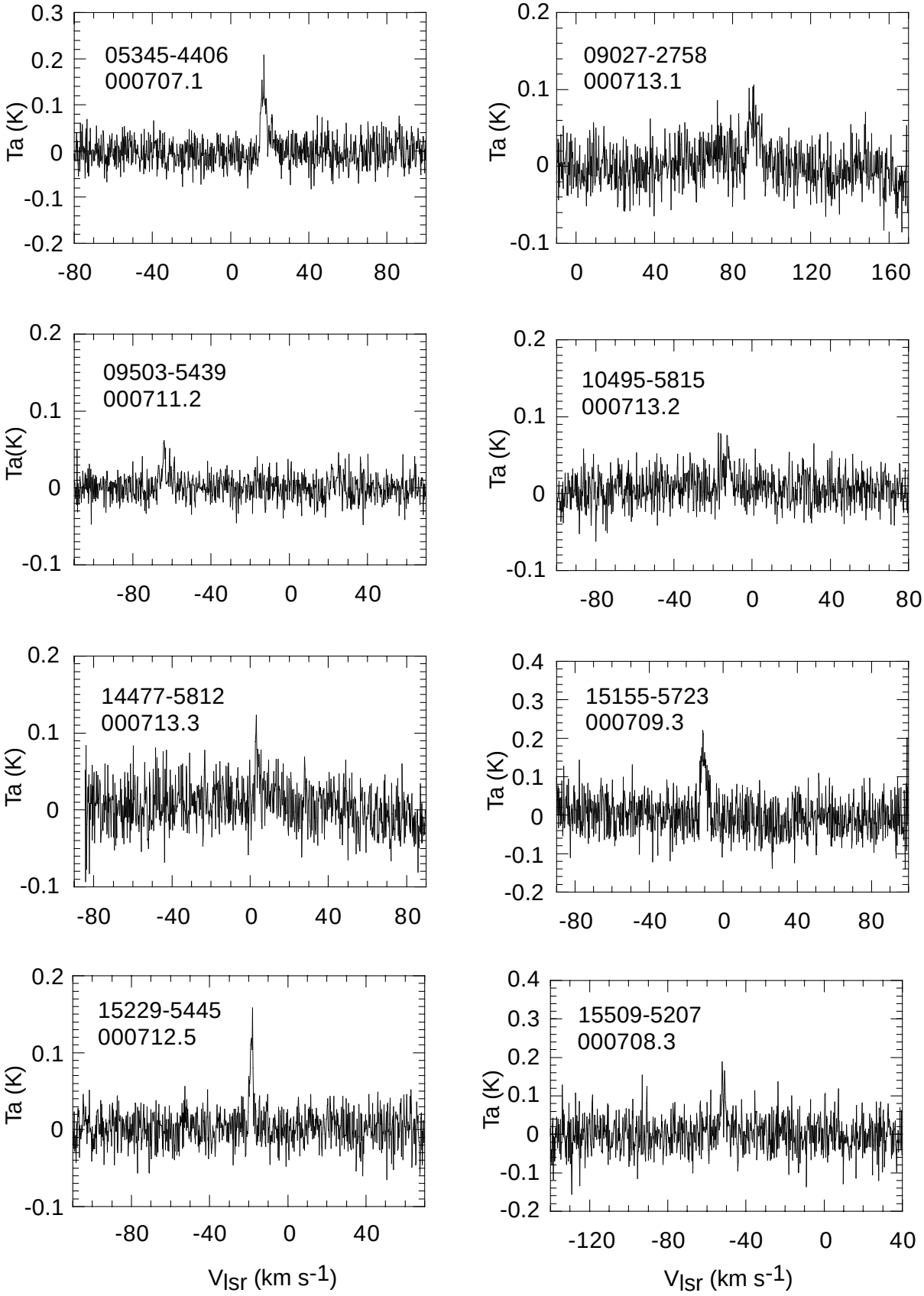

Fig. 1. Spectra of the 24 new detections in the SiO $J = 2–1$ $v = 1$ transition.

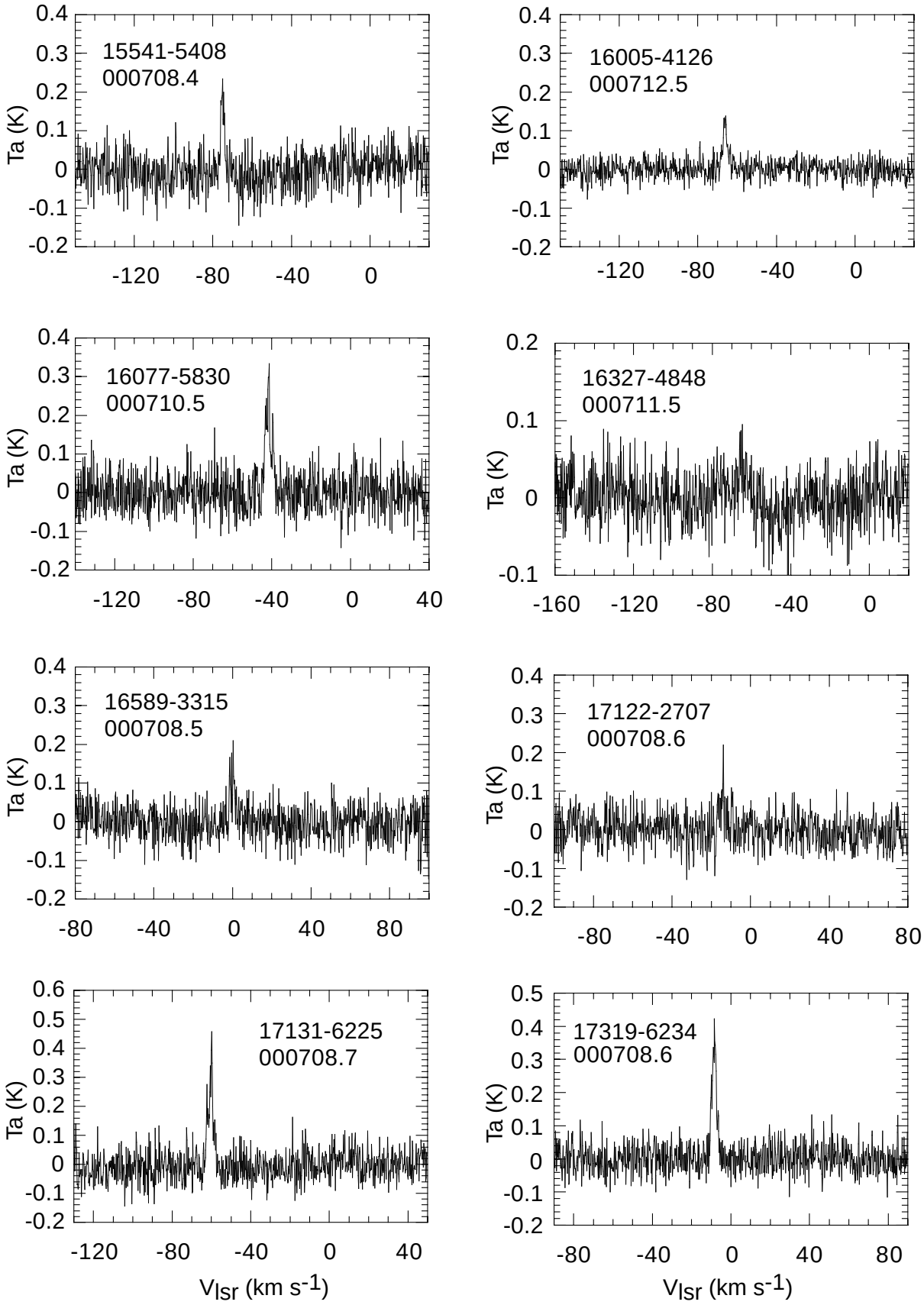

Fig. 1. (Continued)

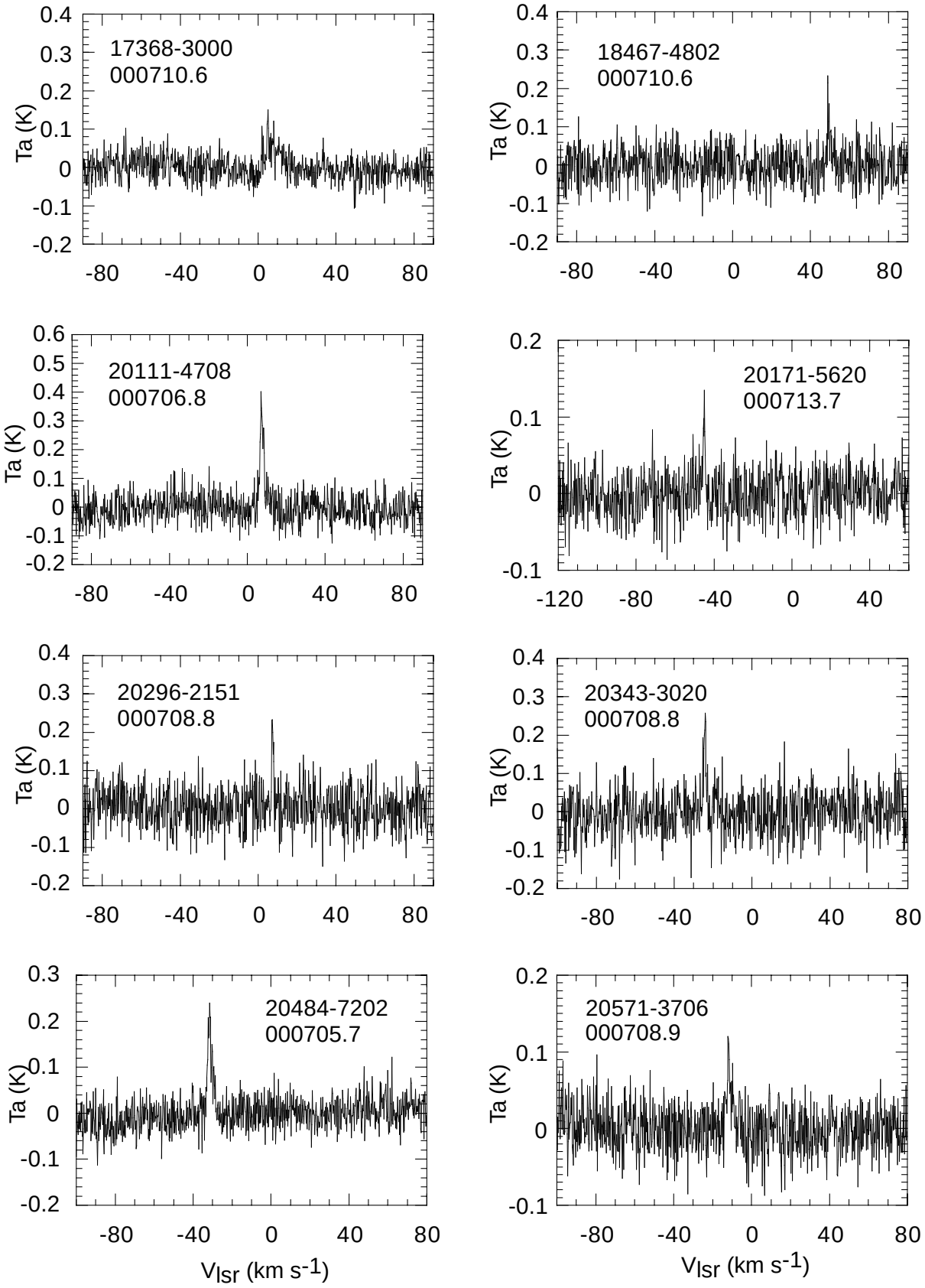

Fig. 1. (Continued)

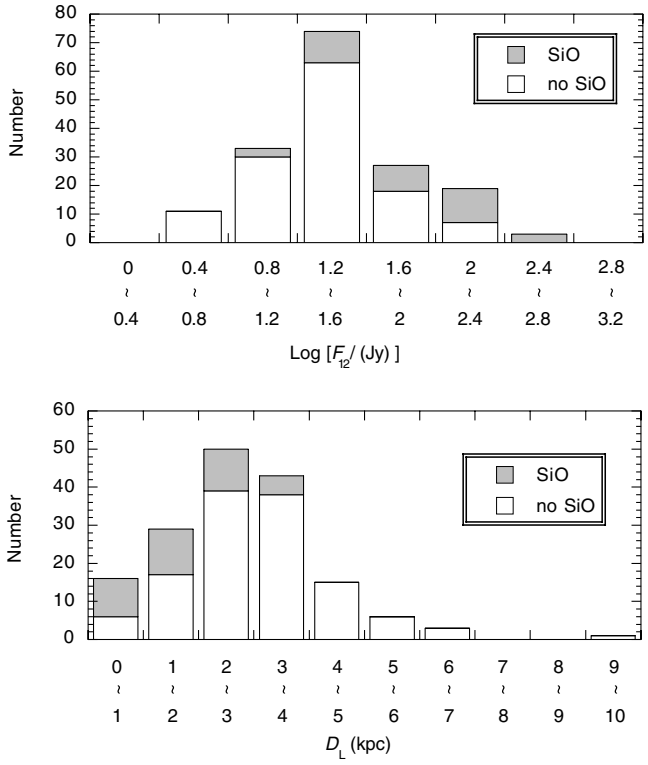

Fig. 2. Histograms of the IRAS 12 micron flux densities (upper panel) and luminosity distances (lower panel) of the observed sources. The detections are shaded.

added). Figure 1 shows the spectra of the 22 new detections. We also include the spectra of 16589−3315 and 17122−2707 in figure 1, because the previous detections were of the SiO J = 1–0 v = 1 and 2 lines at 43 GHz, and these are new detections in the J = 2–1 v = 1 line at 86 GHz.

The observed velocity of the SiO maser line is known to coincide with the stellar velocity (Jewell et al. 1991; Jiang et al. 1995), which is at the middle of the OH 1612 MHz maser double peaks in velocity. We have listed the stellar velocity found in the literature in the 7th column of table 1. We give the middle velocity of the OH 1612 MHz double peaks in this column whenever the OH spectrum is available. The observed SiO velocity coincides with the stellar velocity within a few km s^{-1}, except for a few sources: 05027−2158, 10495−5815, 13203−5536, and 16077−5830. Since the observed velocities of SiO in Haikala (1990) for 05027−2158, and 13203−5536 are consistent with the present observations, it is likely that the OH masers observed by te Lintel-Hekkert et al. (1991) were contaminations from nearby IRAS sources due to the large beam size (about 10′), as noted by Izumiura et al. (1999) for other sources.

The data in the CO J = 1–0 line at 115.271 GHz was simultaneously taken during the first-half period of SiO observations. We seriously checked the CO data; some of the spectra showed strong emission, apparently due to contamination by background molecular clouds in the galactic plane. Because of the position-switching observations, these molecular cloud components often exhibited absorption features in the spectra because of subtraction of emission at the off-position. Among these spectra, we encountered one (only one) curious CO emission feature toward 16146−5257, peaking at V_{lsr} = 92.5 km s^{-1} close to the center velocity of double peaks at 94.5 km s^{-1} (te Lintel-Hekkert et al. 1991; Sevenster et al. 1997b). However, the full width (at the zero intensity) of this CO line is about 10 km s^{-1}, which is much smaller than the width of the OH double peaks, 33.6 km s^{-1}. In addition, the peak temperature of the CO line, T_a = 0.75 K, is too strong for this weak source (F_{12} = 42.6 Jy). Therefore, we discarded this emission as originating in the circumstellar envelope of this star and identified it instead with background molecular clouds. So far, we could not detect any obvious circumstellar CO emission in this survey. We do not discuss CO observations further in this paper.

3. Discussion

3.1. *Properties of the Observed Sources*

Figure 2 shows histograms of F_{12} (upper panel) and the luminosity distance (lower panel). Here, the luminosity distance was obtained from the IRAS flux density, F_{12}, and the color, C_{12}, with the formula for a bolometric correction given in van der Veen and Bruekers (1989), assuming a luminosity of 8000 $L_\odot$ (Vassiliadis, Wood 1993; Deguchi et al. 1999; Nakashima et al. 2000). Figure 2 shows that the detection rate decreases with decreasing flux density, F_{12} (upper panel), and with increasing distance (lower panel). The distance that we can reach in this survey turns out to be about 4 kpc, which is smaller than the distance reached by the corresponding northern SiO survey (with the Nobeyama 45-m telescope; e.g., Deguchi et al 2000ab), or by the OH 1612 MHz survey in the southern galactic plane (ATNF; Sevenster et al. 1997ab).

A two-color diagram for the observed sources is shown in figure 3. Most of the sources have colors of $C_{23} \sim -0.5--1$, which were chosen by the selection criteria. The positions of these stars in the two-color diagram indicate that they are O-rich AGB stars (van der Veen, Habing 1988).

A group of sources near the upper right corner of figure 3 are candidates for protoplanetary nebulae (these are marked "*" in table 2). The colors of these sources are quite similar to the recently found bipolar nebula, IRAS 18312+1950, which exhibits H_2O and SiO maser emissions (Nakashima, Deguchi 2000). We could not detect SiO emission from any of these sources. The IRAS variability indices of these protoplanetary candidates are below 30, while most of the other observed sources are above 95, indicating that flux variations of these protoplanetary candidates are small. Note that this color region has an overlap with those of young stars and protostars embedded in molecular clouds. It is thus possible that these sources are not protoplanetaries at the stage of leaving the AGB phase.

3.2. *Kinematics of the Sources*

Figure 4 shows a longitude–velocity diagram for the SiO detected sources. The open circles represent the detected sources at high galactic latitudes, while the filled circles indicate the detected low-latitude sources. The high-latitude sources are probably located closer to the Sun with less contribution to their radial velocities from the galactic rotation. They are therefore concentrated around V_{lsr} = 0. On the other

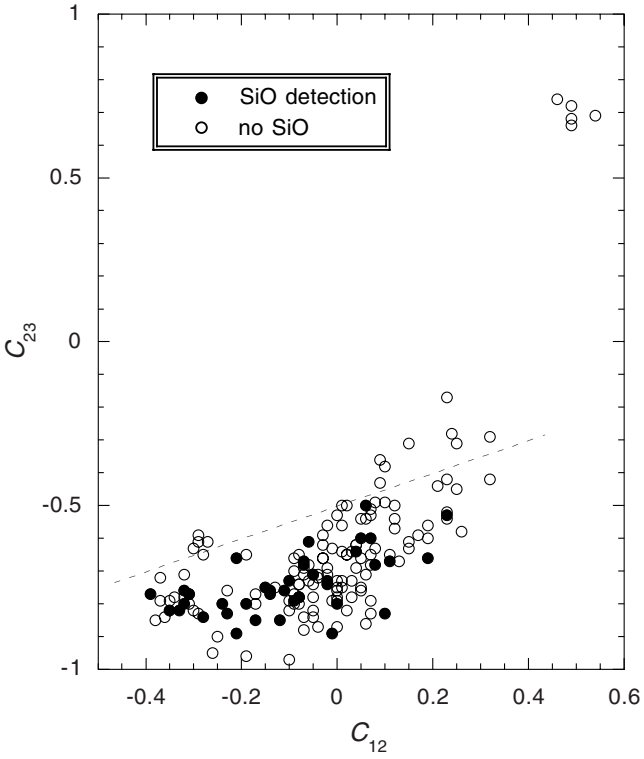

Fig. 3. Two-color diagram of the observed sources, where $C_{23} = \log(F_{60}/F_{25})$ and $C_{12} = \log(F_{25}/F_{12})$. The broken line indicates blackbody emission. The filled and unfilled circles indicate the SiO detection and nondetections, respectively. The sources occupying the upper right corner are candidates for protoplanetary nebulae.

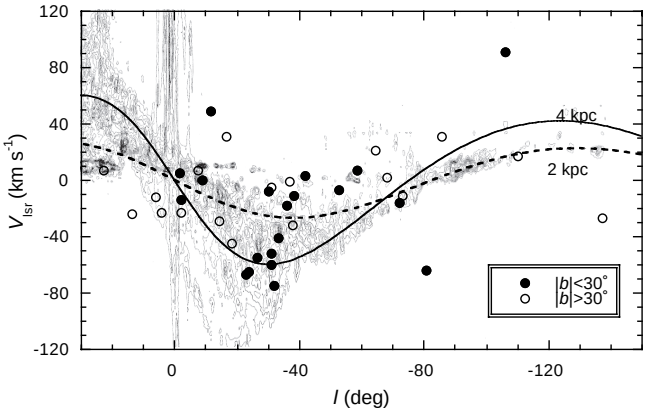

Fig. 4. Longitude–velocity diagram for the detected sources. The filled and unfilled circles indicate the sources at low ($|b| < 30^\circ$) and high ($|b| > 30^\circ$) galactic latitudes. The broken and solid curves indicate the velocities expected from the galactic rotation curve (~ 200 km s^{-1}; nearly flat curve) at distances of 2 and 4 kpc, respectively, from the Sun. The CO l–v map in Dame et al. (1987) was overlayed.

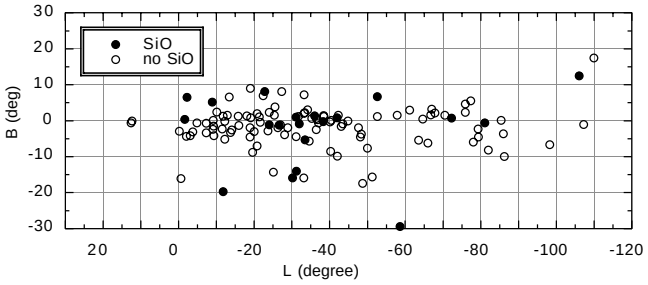

Fig. 5. Source distribution near the galactic plane below $|b| < 30^\circ$. The filled and unfilled circles indicate SiO detections and nondetections, respectively. A relatively large concentration of the detected sources is seen in the range $-45^\circ < l < -25^\circ$.

hand, the sources with $|b| < 30^\circ$ (the filled circles), spreading more at the negative longitudes,[3] would include more distant sources, and are consistent with the expected galactic rotation drawn as the solid and broken curves. In figure 4, one source, 09027−2758, has $V_{lsr} = 91$ km s^{-1} at $l = -107^\circ$, occupying a slightly higher position than the others. Since the estimated distance of this source is approximately 3.6 kpc, the deviation from the galactic rotation is about 50 km s^{-1}, which seems to be within the average deviation in radial velocity from the galactic rotation. From figure 4 and the calculated luminosity distances, we can safely conclude that all the stars which we have detected are within a distance of ~ 4 kpc.

3.2.1. Local velocity dispersion

In order to investigate the structure of the velocity field near the Sun, we computed the local velocity dispersion of stars, i.e., the root mean square of the radial velocities after subtracting the galactic rotation contribution. A nearly flat rotation curve was assumed; see the formula given in the caption of figure 5 in Izumiura et al. (1999). The velocity dispersion is 34.8 km s^{-1} for 20 sources with $|b| < 30^\circ$, and 22.3 km s^{-1} for 18 sources with $|b| > 30^\circ$. We also found similar values for the velocity dispersion (34.7 and 21.8 km s^{-1} for the 91 and 30 sources below and above $|b| = 30^\circ$, respectively) for the IRAS/SiO sample in Haikala (1990) and Haikala et al. (1994). Because the galactic rotation, which depends on the distance, was subtracted from the observed radial velocities, errors in the estimated distances can affect the result significantly. The high-latitude sources which lie relatively closer to the Sun ($\langle D_L \rangle = 1.2$ kpc) suffer less from the errors in the estimated distances than those in the low-latitude sample ($|b| < 30^\circ$; $\langle D_L \rangle = 2.1$ kpc). Of course, it is also possible that the vertical velocity dispersion is somewhat less than the radial dispersion (called U, V, and W components in galactic dynamics; Mihalas, Binney 1981). Taking into account this possibility, we conclude that the local velocity dispersion from the galactic rotation near the Sun is approximately 30 km s^{-1} for the IRAS/SiO sample presented here.

This local velocity dispersion for the IRAS/SiO sample is compatible with the previously obtained values, $\langle u^2 \rangle^{0.5} \sim 30$ km s^{-1} for the disk giants (M-type), and it is appreciably smaller than $\langle u^2 \rangle^{0.5} \sim 50$–80 km s^{-1} found for the optically selected long-period Mira variables (Mihalas, Binney 1981,

[3] (in p. 311) The standard devitations of V_{lsr} (from the average) are 22.6 and 41.8 km s^{-1} for the two groups above and below $|b| = 30^\circ$, respectively. A statistical test (F-test) gives the probablity of about 1% for the null hypothesis of both groups being compatible.

p. 423).

3.2.2. Norma concentration

A relatively large concentration of the SiO detected sources can be seen in figure 4 in the region $l = -25 - -40^\circ$ and $V_{\rm lsr} = -80 - -30$ km s^{-1}. Most of these sources are located close to the galactic plane, as shown in figure 5. This concentration of sources[4] coincides with the direction called "Norma tangent" (Dame et al. 1987), where the line of sight crosses tangentially to the Norma spiral arm at about 8 kpc away. A similar concentration of the OH 1612 MHz sources can be seen at the same position in figures 12 and 13 in Sevenster (1999). This feature is near the edge of the "molecular ring" feature in the CO l–v map (Dame et al. 1987), where an abundant population of the molecular clouds ($R \sim 3$ kpc) exists. The present SiO survey does not reach to sources beyond 4 kpc. In figure 4, in fact, we can find no feature corresponding to the inner structure of the Galaxy, such as a "molecular ring", or a bar. Therefore, the high concentration of SiO sources toward Norma tangent is a phenomenon somewhat nearby to the Sun.

The line of sight toward Norma tangent crosses two spiral arms Sagittarius–Carina and Scutum–Crux arms at the distances of about 2 and 4 kpc, respectively [see naming of arms in Sevenster (1999), or alternatively in Taylor and Cordes (1993) assigning the arms Nos. 3 and 2, respectively]. Considering the average radial velocity of this feature of about -55 km s^{-1}, the kinematic distance to the concentration is about 4 kpc.

Because a high concentration of the OH 1612 MHz sources is also seen at the same position and radial velocity in the l–v diagram in a more sensitive survey (Sevenster 1999), we feared that the concentration of OH 1612 MHz sources might be located far away. We computed the luminosity distances of the 46 OH 1612 MHz sources in this region ($|l - 330| < 10^\circ$ and $|V_{\rm lsr} + 55| < 30$ km s^{-1}) using IRAS F_{12} and C_{12}; a histogram of their luminosity distances is in figure 6. Apparently the OH 1612 MHz sources distribute far beyond 4 kpc because of the high sensitivity of the survey. However, the peak of the OH distribution falls between 3 and 4 kpc, indicating that this peak concentration of the sources is probably on the Scutum arm. The present SiO maser survey reaches this peak, but the feature is present continuously along the line of sight from 1 kpc to 6 kpc. At the opposite side of the galactic longitude, i.e., in $20^\circ < l < 40^\circ$, we do not find any very strong concentrations of sources as Norma, where deeper SiO maser surveys in the SiO $J = 1$–0 $v = 1$ and 2 transitions have been made with the Nobeyama 45-m telescope (Izumiura et al. 1999; Nakashima et al. 2001). At present, the data are biased to the sources at positive galactic longitude in SiO. An original intention of the present work is to remedy the imbalance of SiO sources at the negative longitude side to some degree. If both dual-channel receivers are optimized for single-side band operation at 86.243 GHz, the sensitivity would be improved by a factor of a few, allowing the Mopra telescope to reach sources farther away. This would be useful to remove the imbalance further and to determine whether the SiO masers also show inner galactic structures, such as a "molecular ring" and a bar.

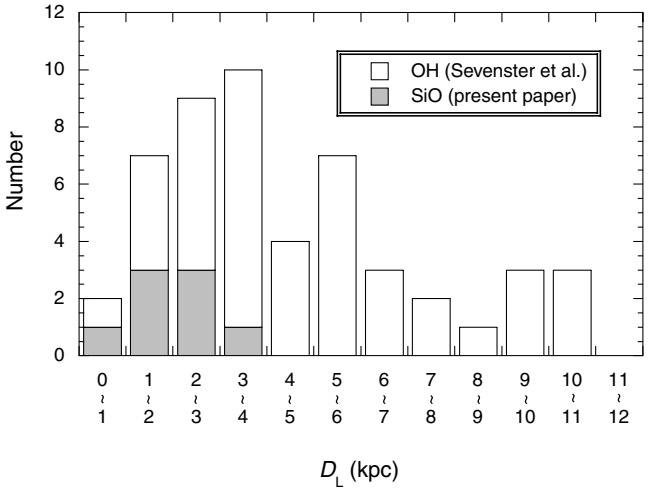

Fig. 6. Histogram of distances for the source sample in the area $|l - 330^\circ| < 10^\circ$ and $|V + 55| < 30$ km s^{-1}. The shaded area is for the present SiO sample, and the blank area for the OH 1612 MHz sources in Sevenster et al. (1997b). Two OH sources at $D_L = 14$–15 kpc are outside of this plot.

4. Conclusion

We have detected 38 SiO maser sources out of 163 observed southern IRAS sources with the Mopra 22-m telescope; 22 SiO detections are new. Among the new detections, 6 sources are without OH detections, and 4 sources have an incorrect OH-velocity assignment. The maximum distance reachable in this SiO survey was found to be about 4 kpc from the Sun, reaching to the Scutum–Crux arm.

We thank the ATNF staff and Michael Murphy, University of New South Wales, for helping with the observations at Mopra Observatory. This research was partly supported by Grant in Aid (c) 20197825 from Japan Society of Promotion of Sciences. This research has made use of the SIMBAD database, operated at CDS, Strasbourg, France.

[4] The l distributions for the SiO-detected and nondetected sources with $|b| < 5^\circ$ are statistically different in the F-test with 99% confidence level; the average and the standard deviation were $321\overset{\circ}{.}5$ and $23\overset{\circ}{.}0$, respectively, for the 10 detected sources and $313\overset{\circ}{.}5$ and $65\overset{\circ}{.}0$ for the 75 nondetections.

References

Allen, D. A., Hall, P. J., Norris, R. P., Troup, E. R., Wark, R. M., & Wright, A. E. 1989, MNRAS, 236, 363

Allen, L. E., Kleinmann, S. G., & Weinberg, M. D. 1993, ApJ, 411, 188

Beichman, C. A., Neugebauer, G., Habing, H. J., Clegg, P. E., & Chester, T. J. 1988, IRAS Catalogs and Atlases, I. Explanatory Supplement, NASA RP-1190 (Washington: US Government Printing Office), VII-22

Dame, T. M., Ungerechts, H., Cohen, R. S., de Geus, E. J., Grenier, I. A., May, J., Murphy, D. C., Nyman, L.-Å., & Thaddeus, P. 1987, ApJ, 322, 706

Deguchi, S., Fujii, T., Izumiura, H., Kameya, O., Nakada, Y., & Nakashima, J. 2000b, ApJS, 130, 351

Deguchi, S., Fujii, T., Izumiura, H., Kameya, O., Nakada, Y., Nakashima, J., Otsubo, T., & Ukita, N. 2000a, ApJS, 128, 571

Deguchi, S., Matsumoto, S., & Wood, P. R. 1999, PASJ, 50, 597

Deguchi, S., Nakada, Y., & Sahai, R. 1990, A&A, 230, 339

Haikala, L. K. 1990, A&AS, 85, 875

Haikala, L. K., Nyman, L.-Å., & Forsström, V. 1994, A&AS, 103, 107

Hall, P. J., Allen, D. A., Troup, E. R., Wark, R. M., & Wright, A. E. 1990, MNRAS, 243, 480

Izumiura, H., Deguchi, S., Fujii, T., Kameya, O., Matsumoto, S., Nakada, Y., Ootsubo, T., & Ukita, N. 1999, ApJS, 125, 257

Izumiura, H., Deguchi, S., Hashimoto, O., Nakada, Y., Onaka, T., Ono, T., Ukita, N., & Yamamura, I. 1994, ApJ, 437, 419

Izumiura, H., Deguchi, S., Hashimoto, O., Nakada, Y., Onaka, T., Ono, T., Ukita, N., & Yamamura, I. 1995, ApJ, 453, 837

Jewell, P. R., Snyder, L. E., Walmsley, C. M., Wilson, T. L., & Gensheimer, P. D. 1991, A&A, 242, 211

Jiang, B. W., Deguchi, S., Izumiura, Y., Nakada, Y., & Yamamura, I. 1995, PASJ, 47, 815

Mihalas, D., & Binney, J. 1981, Galactic Astronomy (2nd ed.: San Francisco: Freeman)

Nakashima, J., & Deguchi, S. 2000, PASJ, 52, L43

Nakashima, J., Deguchi, S., Fujii, T., Izumiura, H., Kameya, O., & Nakada, Y. 2001, ApJ, submitted

Nakashima, J., Jiang, B. W., Deguchi, S., Sadakane, K., & Nakada, Y. 2000, PASJ, 52, 275

Nyman, L.-Å., Hall, P. J., & Olofsson, H. 1998, A&AS, 127, 185

Sevenster, M. N. 1999, MNRAS, 310, 629

Sevenster, M. N., Chapman, J. M., Habing, H. J., Killeen, N. E. B., & Lindqvist, M. 1997a, A&AS, 122, 79

Sevenster, M. N., Chapman, J. M., Habing, H. J., Killeen, N. E. B., & Lindqvist, M. 1997b, A&AS, 124, 509

Taylor, J. H., & Cordes, J. M. 1993, ApJ, 411, 674

te Lintel-Hekkert, P., Caswell, J. L., Habing, H. J., Haynes, R. F., & Norris, R. P. 1991, A&AS, 90, 327

van der Veen, W. E. C. J., & Breukers, R. J. L. H. 1989, A&A, 213, 133

van der Veen, W. E. C. J., & Habing, H. J. 1988, A&A, 194, 125

Vassiliadis, E., & Wood, P. R. 1993, ApJ, 413, 641